Raman Scattering Studies of Solid-Phase Species

D. P. Weaver and J. W. L. Lewis
ARO, Inc.

April 1980

Final Report for Period October 1, 1977 — September 30, 1979

ARNOLD ENGINEERING DEVELOPMENT CENTER
ARNOLD AIR FORCE STATION, TENNESSEE
AIR FORCE SYSTEMS COMMAND
UNITED STATES AIR FORCE

This report has been reviewed by the Office of Public Affairs (PA) and is releasable to the National Technical Information Service (NTIS). At NTIS, it will be available to the general public, including foreign nations.
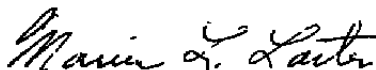
APPROVAL STATEMENT

This report has been reviewed and approved.

KENNETH H. LENERS, Captain, USAF
Project Manager
Directorate of Technology

Approved for publication:

FOR THE COMMANDER

MARION L. LASTER
Director of Technology
Deputy for Operations

REPORT DOCUMENTATION PAGE		READ INSTRUCTIONS BEFORE COMPLETING FORM
1 REPORT NUMBER AEDC-TR-80-4	2 GOVT ACCESSION NO.	3 RECIPIENT'S CATALOG NUMBER
4 TITLE (and Subtitle) RAMAN SCATTERING STUDIES OF SOLID-PHASE SPECIES		5 TYPE OF REPORT & PERIOD COVERED Final Report, October 1, 1977 – September 30, 1979
		6 PERFORMING ORG. REPORT NUMBER
7 AUTHOR(s) D. P. Weaver and J. W. L. Lewis, ARO, Inc., a Sverdrup Corporation Company		8 CONTRACT OR GRANT NUMBER(s)
9 PERFORMING ORGANIZATION NAME AND ADDRESS Arnold Engineering Development Center/DOT Air Force Systems Command Arnold Air Force Station, Tennessee 37389		10 PROGRAM ELEMENT, PROJECT, TASK AREA & WORK UNIT NUMBERS Program Element 65807F
11. CONTROLLING OFFICE NAME AND ADDRESS Arnold Engineering Development Center/DOS Air Force Systems Command Arnold Air Force Station, Tennessee 37389		12 REPORT DATE April 1980
		13. NUMBER OF PAGES 39
14 MONITORING AGENCY NAME & ADDRESS(If different from Controlling Office)		15. SECURITY CLASS. (of this report) UNCLASSIFIED
		15a DECLASSIFICATION/DOWNGRADING SCHEDULE N/A

16 DISTRIBUTION STATEMENT (of this Report)

Approved for public release; distribution unlimited.

17 DISTRIBUTION STATEMENT (of the abstract entered in Block 20, If different from Report)

18. SUPPLEMENTARY NOTES

Available in DTIC

19 KEY WORDS (Continue on reverse side if necessary and identify by block number)

Raman spectroscopy	temperature	ammonium nitrate
scattering	polystyrene	carbon dioxide
solid phases	lasers	
spectra	substrates	
cryopumping	sodium nitrates	

20 ABSTRACT (Continue on reverse side if necessary and identify by block number)

The Raman spectra of cryosorbed samples of CO_2, CO, N_2, O_2, CH_4, NH_3, and H_2O were obtained. Cryodeposit thickness was nominally 10 to 11 μm, and sample temperatures were systematically varied over the range of 17 to 85 K. Spectral scans were obtained for both the lattice mode region (25 to 200 cm^{-1}) and intra-molecular vibrational mode region (200 to 4,000 cm^{-1}). Additionally, the Raman spectra of single polystyrene latex spheres

DD FORM 1473 1 JAN 73   EDITION OF 1 NOV 65 IS OBSOLETE

20.   ABSTRACT (Continued)

0.220 μm in diameter and bulk, powdered samples of inorganic particles of $NaNO_3$ and NH_4NO_3 were recorded.   The dependence of the Raman scattering signature of $NaNO_3$ on sample temperature and the spectral variations as a function of change in concentration of a sample formed from a mixture of $NaNO_3$ and NH_3NO_3 were investigated.

AFSC
Arnold AFS Tenn

PREFACE

CONTENTS

ILLUSTRATIONS

Figure

TABLES

1.0 INTRODUCTION

The potential contamination of spacecraft system surfaces by the exhaust effluents of various rocket engine sources has resulted in a need for the development of a variety of contamination diagnostics. Of particular interest in this regard are those measurement techniques which are applicable for use in ground-based simulation facilities. Further, it is necessary to provide remote measurement capabilities for the determination of the species present within a contaminant deposit, and, of course, the techniques should exhibit molecular specificity. Additional requirements of such methods of measurement include the capability for providing spatial resolution and an inherent speed of measurement which is sufficiently great to enable the detection of time variations in the nature of the contaminant deposit throughout the exhaust period of a rocket engine. Raman scattering is one technique which appears to satisfy these requirements and is nondestructive in its operation, a feature which allows subsequent studies to be performed without previous sample degradation. Moreover, the technique not only possesses molecular specificity but is not restrictive in the type of molecules which are detected; i.e., both homonuclear and heteronuclear diatomic species as well as polyatomic species are detected.

A determination of the applicability of Raman scattering as a contaminant diagnostics technique requires consideration of the type or source of the contaminant deposit. Clearly, two distinct types of deposition processes can be operative in a given engine exhaust: (1) particles formed in the combustion expansion processes can be deposited and collected on the solid surfaces located in the exhaust region, and (2) molecular species within the exhaust plume can be cryopumped or adsorbed onto the surface material if the surface temperature is sufficiently low. These two different mechanisms produce quite distinct contaminant deposits in that the particulate source deposit will consist of discrete, discontinuous material deposits which, under microscopic examination, are capable of distinction. In contrast, molecular species contamination can result in a near-crystalline, macroscopically continuous deposit. If generally applicable, Raman scattering should provide species constituency information for both types of deposition or contamination and, in particular, yield constituency information of single contaminant particles.

To assess the applicability of Raman scattering to the problem of contaminant diagnostics, an experimental study has been conducted in which scattering measurements have been performed on cryopumped molecular species as well as powdered, particulate samples. The following sections of this report both describe these efforts and assess the status of the applicability of Raman scattering as a diagnostics technique for contamination studies.

2.0 DESCRIPTION OF SOLID-STATE RAMAN SCATTERING

The interaction of monochromatic radiation with molecular species is known to result in scattering of the incident radiation, and the scattered radiation is found to include components which have been shifted in wavelength (or frequency) with respect to the wavelength (λ_o) of the incident radiation. Raman scattering is one of the processes which produces such wavelength-shifted components, and if the induced polarization of the sample varies linearly with the incident electric field, the process is defined to be spontaneous Raman scattering (RS). Considering only the RS process, it is found that the scattered radiation is both up- and down-shifted relative to λ_o, and such components are denoted as Stokes and anti-Stokes scattering, respectively. This qualitative description of the Raman process is applicable to solid-, liquid-, and gaseous-phase molecular species, and the Raman components result, in the classical interpretation, from a modulation of the incident radiation by the characteristic motions of the scattering species. Clearly, there are differences to be expected in the nature of the Raman components for a given molecular species of different phases, for in the transition from the gaseous to the solid phase a suppression of the characteristic rotational motion occurs. However, if the intermolecular binding is neither ionic nor covalent in nature, the intramolecular binding energies greatly exceed the intermolecular binding energy. Consequently, for such solid lattices or structures, there is but little difference found for the values of the characteristic, intramolecular vibrational frequencies upon solidification of the molecular species. Of course, solidification can result in the removal of various symmetries of the molecular species, and degenerate vibrational modes can be split. For such cases, the mean energy of the yet remaining, degeneracy-weighted energy eigenvalues of the split levels is that of the unperturbed, degenerate levels. As a result of these considerations, for weakly bound species, which are typical of cryodeposits, the molecular species exhibit Raman scattering frequency shifts which are closely related to the corresponding gas-phase spectra, the result of which is to enable indentification of the solid-phase species.

Further, intermolecular, collective motion of the solid phase results in additional characteristic frequencies for the lattice or structure. Consequently, for the majority of lattices and structures the totality of the characteristic frequencies can be categorized as either lattice modes, corresponding to the intermolecular, collective degrees of freedom, or vibrational modes, corresponding to the intramolecular degrees of freedom.

Having presented a qualitative description of the gross characteristics of Raman scattering from a solid species, a mathematical representation of some of the more simple aspects of the scattering process for a single species lattice or structure will be useful. Consistent with the assumption of weak coupling between the intermolecular and

intramolecular modes of motion of the solid structure, the Hamiltonian (H) of the structure is separable into lattice and intramolecular components, i.e.,

$$H = H_L + H_v \tag{1}$$

where the lattice and intramolecular vibrational operator components are denoted by H_L and H_v, respectively. Consequently, using Dirac notation, the total eigenfunction $|\Psi\rangle$ can be written as a product of the eigenfunctions of the lattice and intramolecular modes

$$|\Psi\rangle = \prod_\ell |\psi_\ell\rangle \prod_v |\psi_v\rangle \tag{2}$$

In the semiclassical approximation for the Raman scattering process, it can be shown (Ref. 1) that the scattered intensity is proportional to the square of the transition matrix element for the polarization vector $\vec{P}$; i.e.,

$$I \sim \overline{|\langle f|\vec{P}|i\rangle|^2} \tag{3}$$

where $|f\rangle$ and $|i\rangle$ represent the final and initial state and thermal averaging is denoted by the bar. Further, $\vec{P}$ is related to the incident electric field of amplitude E_o by contraction of the second-rank polarizability tensor $\underline{\alpha}$ and $\vec{E}_o$, i.e.,

$$\vec{P} = \underline{\alpha} \cdot \vec{E}_o \tag{4}$$

Neglecting higher-order Raman processes, a first-order Taylor series expansion of $\underline{\alpha}$ in the set of normal coordinates or displacement vectors $\{Q_k\}$ yields

$$\underline{\alpha} = (\underline{\alpha})_o + \sum_k \left(\frac{\partial \underline{\alpha}}{\partial Q_k}\right)_o Q_k \tag{5a}$$

$$= (\underline{\alpha})_o + \sum_k (\underline{\alpha}')_k Q_k \tag{5b}$$

where the subscript o denotes evaluation at the equilibrium position of the lattice or structure and the derived polarizability tensor $\underline{\alpha}'$ is defined to be

$$\underline{\alpha}' = \left(\frac{\partial \underline{\alpha}}{\partial Q_k}\right)_o \tag{6}$$

A further simplification results by the decomposition of $\{Q_k\}$ into the complementary sets of $\{Q_m^{(\ell)}\}$ and $\{Q_n^{(v)}\}$, where the superscripts ℓ and v denote lattice modes and intramolecular vibrational modes, respectively. Consequently, Eq. (5b) can be written as

$$\underline{\alpha} = (\underline{\alpha})_0 + \sum_m \left(\underline{\alpha}'^{(\ell)}\right)_m Q_m^{(\ell)} + \sum_n \left(\alpha'^{(v)}\right)_n Q_n^{(v)} \tag{7}$$

where the derived polarizability of Eq. (6) is specialized in Eq. (7) to the lattice modes, $\underline{\alpha}'^{(\ell)}$, and to the intramolecular vibrational modes, $\underline{\alpha}'^{(v)}$. Additionally, Eqs. (23.3) and (39.14) of Born and Huang (Ref. 2) define the normal coordinates and derived polarizability parameters in terms of the lattice or structure parameters.

Using the results of Eqs. (2), (4), and (7), the transition matrix element for the polarization $\vec{P}$ can be written as

$$\sum_m \left(\underline{\alpha}'^{(\ell)}\right)_m <\Psi_{\ell_f} | Q_m^{(\ell)} | \Psi_{\ell_i}> + \sum_n \left(\alpha'^{(v)}\right)_n <\Psi_{v_f} | Q_n^{(v)} | \Psi_{v_i}>$$

where the Rayleigh scattering condition $|f> = |i>$ has been excluded. The scattered intensity I is found to consist of the following lattice and intramolecular mode components

$$I \sim \overline{\left| \sum_m \left(\underline{\alpha}'^{(\ell)}\right)_m <\Psi_{\ell_f} | Q_m^{(\ell)} | \Psi_{\ell_i}> \right|^2} + \overline{\left| \sum_n \left(\alpha'^{(v)}\right)_n <\Psi_{v_f} | Q_n^{(v)} | \Psi_{v_i}> \right|^2} \tag{8}$$

where combination transitions corresponding to simultaneous transitions in the lattice and intramolecular modes are ignored; i.e., only fundamental transitions are of interest. Further, the requirement for thermal averaging is indicated by the bar symbol in Eq. (8). For such fundamental transitions it is known that in the harmonic oscillator approximation the following selection rules apply (Ref. 1):

$$v_f = v_i \; ; \; \ell_f = \ell_i \pm 1 \begin{Bmatrix} \text{Stokes} \\ \text{anti-Stokes} \end{Bmatrix} \text{lattice mode scattering} \tag{9a}$$

and

$$\ell_f = \ell_i \; , \; v_f = v_i \pm 1 \begin{Bmatrix} \text{Stokes} \\ \text{anti-Stokes} \end{Bmatrix} \text{intramolecular mode scattering} \tag{9b}$$

8

Further, energy conservation requires that the scattered and incident photon frequencies ω and ω_0, respectively, be related according to

$$\omega = \omega_0 \mp \begin{Bmatrix} \omega_{\ell_f \ell_i} \\ \omega_{v_f v_i} \end{Bmatrix} \tag{9c}$$

where the ordering ($\mp$) corresponds to $\begin{pmatrix} \text{Stokes} \\ \text{anti-Stokes} \end{pmatrix}$ scattering, and the energy differences involved in the lattice mode and intramolecular mode transitions are $\hbar\omega_{\ell_f \ell_i}$ and $\hbar\omega_{v_f v_i}$, respectively. Again, in the harmonic oscillator approximation $\omega_{\ell_f \ell_i} = \omega_\ell$ and $\omega_{v_f v_i} = \omega_v$, regardless of the quantum numbers.

For well-defined lattices and structures, further simplification is afforded by the use of group theoretical methods for both the enumeration of the modes of motion of each type (lattice and intramolecular) and symmetry species and the determination of the operative selection rules for each individual mode. Regarding these selection rules, it is to be noted that Eqs. (9a) and (9b) represent necessary but not sufficient constraints in that the symmetry properties of the derived polarizability or the polarizability may be such as to preclude the participation in the Raman process of individual modes of motion (Ref. 1).

From this simplified, heuristic treatment of solid-species scattering it is seen that species identification of the cryodeposit is made possible by the determination of the frequency differences $|\omega_\ell$ and $\omega_v|$ which are characteristic of the molecular species comprising the cryodeposit. Furthermore, although not explicity shown, the thermal averaging required by Eq. (8) implies the existence of a temperature dependence of the scattered intensity which provides a means for determining the cryodeposit temperature. Although it is not difficult to extend the mathematical representation of the existing theory for a single species lattice/structure to include weakly interacting binary and ternary mixtures, the utilization of such a theory requires knowledge of the cryodeposit structure and molecular configuration as well as the details of the intermolecular potential functions. Such information is at present lacking, and, as a result, no practical purpose would be served by such a theoretical development. Similarly, it should be noted that for many contamination cryodeposits encountered in practice no spatially regular lattice/structure configuration exists because of nonuniformity in deposition conditions and crystalline fracturing which can occur as a result of thermal variations and stresses within the cryodeposit. Because of these considerations, for the feasibility study it is considered to be ill advised to pursue further Raman scattering

processes of perfect crystalline lattices. The course of action which is suggested to be indicated is the combined use of existing theoretical developments, when applicable, to provide semiquantitative bases for prediction and interpretation of the Raman scattering results and, although inadequately understood, empirical results of the temperature and concentration dependencies of scattering signals from solid samples of known constituencies, temperatures, and deposition or preparation conditions, even though the solid structure is not adequately known.

In this spirit, it is noted that the Raman band intensities, widths, and frequencies all depend upon temperature. As the temperature of the scattering source is increased the Raman linewidths increase, and there is, in general, a shift to lower frequency (Ref. 3). The form of the equation for the scattered intensity is given by (Ref. 3).

$$I(\nu) = S\frac{\Gamma}{\left(g(\nu,\nu')-\Delta\right)^2 + \Gamma^2} \tag{10}$$

where I represents the total Raman scattered intensity, $g(\nu,\nu')$ is a function of both incident and scattered frequencies, Δ is the shift in frequency of the Raman line at frequency ν, and the half width is given by Γ. In most cases the shift Δ and half-width Γ, which depend upon anharmonic forces of the lattice (Ref. 4), involve complex expressions which require numerical evaluation.

Concerning the temperature dependence of the integrated intensity of a Raman band resulting from solid species, although few experimental studies have been performed, it can be concluded that at present the results are varied and inconclusive (Refs. 5 and 6). However, the ratio of the integrated intensities of anti-Stokes and Stokes scattering is, to first order, given by

$$\frac{I(\text{anti-Stokes})}{I(\text{Stokes})} \cdot \exp\left(\frac{-\hbar\omega_{r,s}}{k_B T}\right) \tag{11}$$

The temperature variation of the vibrational frequencies of solid samples involves a mixed dependence on both temperature and volume. As noted above (Refs. 3 and 5), a decrease in temperature increases the frequencies. This effect is associated with the decrease in the intermolecular distance because of the contraction of the crystal lattice on cooling. This frequency shift is observed to be nearly linear with temperature, changing but slightly at low temperatures. Further, as expected, compression of the sample produces variations in the Raman signal which are similar to those observed for sample cooling (Ref. 7).

The widths of Raman lines (primarily low-frequency) have also been studied (Refs. 8 and 9). Here, increases in bandwidth are observed to occur as temperature increases. Broadening of the bands in the low-frequency spectra is associated primarily with the anharmonicity of the vibrational modes and sudden changes in the orientation of molecules. Clearly, then, the most useful characteristic of the band intensity is the integrated intensity.

The variation of band positions and intensities in mixtures as a function of concentration can also provide valuable information about the effect of molecular interactions on the Raman spectra. In the absence of molecular interaction, the line intensities are proportional to the number of scattering molecules, and, specifically, to the volume concentration c of the scattering component in the mixture

$$I = Kc \qquad (12)$$

where K is a constant. The linear dependence of I on the concentration c of a species in a solid mixture is a rather special condition which can be approached only in the near-ideal lattice or structure. Specifically, the validity of Eq. (10) requires, in general, additivity of the specific volumes of the mixture species, independence of the species' molecular polarizability of the mixture constituency, and, obviously, the absence of spectral overlap of the Raman signals of the various species of the mixture (Ref. 10).

Further, nonlinear dependence of the intensity of Raman lines on the concentration of the scattering molecules occurs as a result of the formation of solid-state molecular compounds (Ref. 9). Experimentally it is found that two different characteristic types of behavior occur in such mixed crystals (Ref. 3). If, for example, a compound $A_{1-x}B_xC$ is formed from AB and BC each of which has one optically active mode, ν_A and ν_B, respectively, the two possible forms may be characterized.

Single-mode, mixed crystals continue to show a single optical mode that shifts linearly with concentration x from the frequency ν_A, to ν_B. The linewidth increases and typically has a maximum for a 1:1 mixture, e.g., x = 0.5, and the integrated intensity of the Raman line for such compounds does not change appreciably with concentration.

Two-mode, mixed samples, on the other hand, show two modes of vibration with frequencies close to ν_A and ν_B of the pure compounds. The intensity of the Raman scattering from these modes, however, is proportional to the fraction of each compound present. As the concentration x increases, the intensity of ν_B increases while that of ν_A decreases. In some mixture cases, it is possible for different modes to display different behaviors. Some

theoretical work performed on well-formed crystal structure samples has shown the ability to predict one-mode or two-mode crystal behavior as well as the dependence of the optic mode frequencies on the concentration (Ref. 11).

In the application of Raman scattering techniques to the study of disperse media, such as polycrystalline samples, powders, amorphous cryodeposits, and discrete particles, problems not generally encountered in the study of well-defined crystal lattices are present. It must be recognized that the Raman line intensities are complex function of the material parameters as well as such charcteristics of the disperse medium as grain size. For the case of a contaminating cryodeposit, the sample may be considered as composed of a multitude of grains for which the number per unit volume is so large that scattering by grain boundaries and absorption may be treated as continuous functions of layer thickness. The primary problems that must be recognized in this case are sample heating as a result of absorption of the laser radiation, changes in material properties under cooling, and the disappearance of lower-lying Raman lines attributed to the amorphous nature of the sample's crystal structure. For the case of a discrete particle (of a size comparable to or smaller than the wavelength of the incident light) the effects of particle size and shape upon the characteristic features of the Raman spectrum must be considered. In application of the technique, a more important concern, perhaps, will be the interference of surface contamination as the particle surface-to-volume ratio becomes large. Further, the effects of sample heating caused by source radiation must be considered.

3.0 EXPERIMENTAL APPARATUS AND PROCEDURE

Both cryodeposits and powdered particulate samples were studied, and the experimental configurations which were utilized differed for each type of sample. The two experimental configurations employed are shown schematically in Figs. 1 through 4. Although both systems utilized a conventional Raman spectrometer to diperse the characteristic Raman spectra and to reject the Rayleigh-scattered component, the sample production and maintanance methods differed markedly for the two types of samples studied. For the cryodeposit system, spectra were obtained from cryodeposits produced by the condensation of pure gas samples on a cryogenically cooled optical surface which was located within a high-vacuum chamber. For the higher-temperature particulate study, Raman spectra were obtained from not only bulk solids and their mixtures but also from discrete solid particles of diameters as small as 0.220 μm. Additionally, the variations of such spectra with both mixture concentration and sample temperature were obtained from the solid samples which were exposed to the ambient atmosphere.

3.1 Low-Temperature Cryodeposit System

A detailed description of the experimental apparatus including the vacuum chamber, the effusive gas source, and the optical substrate has been presented in Ref. 12; therefore, only a summary of this apparatus is presented in this report. A schematic representation of the experimental apparatus is presented in Fig. 1 which shows the spectrometer, laser source, and the high-vacuum chamber (which contains the cryogen-cooled substrate). The stainless steel chamber was equipped with a liquid-nitrogen-cooled inner liner. The base pressure of the chamber was approximately 10^{-8} torr, and this pressure was maintained following deposition of the sample. However, it should be noted that during the deposition of the sample onto a substrate of 20 K nominal temperature, the chamber pressure increased to approximately 10^{-6} torr. The substrate holder, which is shown in Fig. 2, was actively cooled with either liquid nitrogen (78 K) or nominally 20 K gaseous helium. The temperature of the germanium (Ge) substrate holder was determined to within ± 0.25 K by three platinum resistance thermometers which were located on the holder. Shown in Fig. 2 is a 4-mm-thick Ge window with a 50.8-mm clear aperture which was mounted in the holder for cryogenic cooling.

Controlled deposition onto the cold germanium surface was accomplished with the gas injection system shown schematically in Fig. 3, and a cryodeposit of uniform thickness over the surface was obtained. A toroidal-shaped gas reservoir with thirty-six, equally spaced 1.59-mm-diam orificies directed the pure gas, nominally effusive, source flow toward the Ge substrate. The reservoir pressure was measured using an MKS Baratron® transducer, and the gas flow rate, or deposition, was regulated and controlled by a variable leak valve. The cryodeposit thickness was monitored using a dual-angle interference technique which is described in detail in Ref. 13. The particular technique used two, low-power He-Ne ($\lambda = 6328$ Å) laser beams which were injected into the vacuum chamber and specularly reflected from the Ge substrate at two accurately measured angles. As the cryodeposit formed, the two interference patterns of different periodicity were observed and monitored at the reflected laser angles. Using the ratio of the spatial periods of the interference patterns, the assumed-known refractive index of the crydeposit, and the injection angles (18° and 68°) of the beams, the thickness of the cryodeposit was determined. This dual-beam thickness monitor yielded cryodeposit thickness valves which were accurate to ± 2 percent. While Raman data were obtained from cryodeposit thickness less than 1 μm, typical sample thicknesses for the data presented in this report were between 10 and 11 μm.

A 0.85-m focal length, Spex Model 1401 double monochromator was used in the experiments to disperse the scattered radiation. This double monochromator utilized two 1,200 line/mm gratings. The scattered radiation was detected by a cooled, EMI 9502

photomultiplier tube with an S-20 spectral response. Standard photon counting electronics consisting of a preamplifier/amplifier discriminator combination and rate meter and strip-chart data registration were used. A more detailed description of this counting system is given in Ref. 14.

The collection optics system, shown in Fig. 1, included a 20-cm focal length, f/5 collection lens and a 27.9-cm focal length focusing lens which projected onto the entrance slit of the f/7 monochromator, an image of the scattering region with a magnification factor of 1.4

The laser source was a Coherent radiation Model CR-5 argon-ion laser which was operated at a nominal power level of 100 mW at 5,145 Å. To eliminate the plasma emission lines of the laser, the laser beam was directed through a bandpass interference filter which had a 10 Å full-width, half-maximum transmission window. The beam then transversed a 25:1 beam expander, the output of which filled the aperture of the 100-cm focal length focusing lens which provided an injection beam cross section which could be matched to the collection optics volume.

The acquisition of Raman spectra from the cryodeposit samples was initiated by the evacuation of the vacuum chamber to approximately 10^{-7} torr; both diffusion pumping and cryogenic pumping, using 78 K LN_2, were employed. Next, the Ge substrate, the holder, and the transfer lines were cooled to approximately 20 K using a GHe cryostat, and a vacuum chamber base pressure of approximately 10^{-8} torr was obtained. With the germanium substrate normal to the centerline direction of the effusive source, samples of research grade test gases were introduced into the chamber. Deposition of the gas onto the cold germanium window was monitored with the dual-beam interference technique, and the flow was terminated upon obtaining the desired cryodeposit thickness. The germanium substrate was then rotated so that the sample surface was normal to the collection optics path, and, for this configuration, the laser incidence angle was 67° with respect to the normal to the surface. At this point, Raman scattering spectra were recorded. Upon completion of a spectral scan, the cryogenic flow rate was varied and the process repeated at a different sample temperature. Upon completion of the acquisition of the Raman spectral scans of the sample, the cryogenic fluid flow to the sample was terminated, thereby allowing the substrate and cryodeposit temperatures to increase. When the cryodeposit was completely sublimated, a background scan of the germanium substrate was made for reference purposes.

3.2 Discrete Particulate and Bulk Solid Sample System

The experimental configuration for the study of the powdered particulate samples is shown in Fig. 4. The laser source and Raman spectrometer systems were essentially the same as that used for Raman measurements of cryodeposits. A 0.5-m Spex Model 1301 double monochromator with two 1,200 lines/mm ruled gratings was used for these experiments. A cooled RCA C31034A photomultiplier tube with an S-20 spectral response and standard photon counting electronic processing, as described in the above section, were used. The Raman spectra were recorded using a strip-chart recorder.

The collection optics system was, as before, matched to the monochromator. An f/1.75 collection/focusing lens of 10.2-cm focal length collected the scattered radiation and focused the magnified image (4X) of the scattering volume onto the entrance slit of the spectrometer. The incident laser beam was again passed through a narrow-band interference filter to eliminate plasma emission lines. The slightly expanded laser beam then traversed a 2.54-cm focal length lens which provided a focal diameter of approximately 50 μm. A Coherent Radiation Model CR-5 argon-ion laser was used as the laser source and a laser power of approximately 100 mW at 5,145 Å was used.

Two sample holders were used for this set of experiments. When Raman spectra from discrete, small particles were desired, sample particles were deposited onto a clean glass substrate. For studies of the temperature and concentration variation of Raman spectra of bulk solid samples, the sample was pressed into a conical depression which had been drilled into the end of a 47.5-watt heating element. This arrangement had the advantage of minimizing substrate interference while providing adequate sample heating. To provide measurement and control of the sample temperature, a copper-constantan thermocouple was attached to the base of the conical depression. Sample heating and control in the range of 290 to 550 K with a ±2 K resolution was provided by this means. Both the glass substrate and the sample heating device were capable of attachment to a mounting device which permitted precise three-dimensional positioning of the focal volume with respect to the optical axis of the spectrometer. The laser incidence angle in both cases was maintained so that a normal to the sample surface made an angle of 30° with the axis of the incident laser beam in the plane defined by the incident laser beam and the Raman collection axis.

The reagent grade (99.9-percent minimum purity) materials used in the concentration and temperature variation experiments were ground into a fine powder and pressed into the inverted cone sample holder depression. The exposed sample surface was pressed so that it

was uniformly flat across the 1/8-in. (3 mm)-diam sample face. Mixture samples were prepared by thoroughly mixing measured quantities of pure samples and then pressing the samples into the sample mount. The polystyrene latex sphere samples used for studies of discrete particles were obtained commercially from the Dow Chemical Company and were essentially monodisperse with an individual particle diameter of 0.220 μm.

The technique employed for the dispersion onto the glass substrate of these small particles made use of a dilute dispersion of the particle samples in a particulate-free and chemically pure, volatile organic solvent. A small portion of the dried particle sample was added to 150 m° of the dispersing liquid, methanol, and then placed in an ultrasonic bath The substrate was then immersed in the acoustically vibrated dispersion for a period of 60 sec. After deposition, the sample was subjected to a brief period of vacuum drying in a desiccator. Residual traces of the methanol were not observed in the raman spectra of the particles deposited from this liquid.

4.0 RESULTS AND DISCUSSION

4.1 Cryodeposit Results

The Raman spectra of cryosorbed samples of CO_2, CO, N_2, O_2, CH_4, NH_3, and H_2O were obtained using a cold germanium substrate whose temperatures were systematically varied over the range of 17 to 85 K. All cryodeposits utilized in this study were nominally uniform across the spatial extent of the substrate, and the sample thickness was in the range of 10 to 11 μm. Utilizing an incident laser wavelength of 19, 436 cm^{-1} (5,145 Å), spectral scans were obtained for Raman scattering from both the lattice mode region (25 to 200 cm^{-1}) and intramolecular vibrational mode region (200-4,000 cm^{-1}). The observed Raman band locations for the molecular species studied and the cryodeposit substrate temperatures corresponding to these observations are listed in Table I.

Typical of the laser-excited spectra of these condensed samples was the Raman scattering signature obtained from CO_2 at 83 K, and the lattice mode region of this spectra is reproduced in Fig. 5. As shown by Cahill and Leroi (Ref. 15), CO_2 crystallizes in a face-centered-cubic (FCC) lattice structure, and the corresponding space group is Pa3 (T_h^6); a description of the Hermann-Mauguin and Schoenflies space group nomenclature is given in Ref. 16. Further, the primitive cell contains four CO_2 molecules which are situated on S_6 sites and the molecular axes are parallel to the body diagonals of a cube. For the CO_2 structure, the application of group theory shows that there exist four translational frequencies of species T_u which are IR active and Raman inactive. Further, there exist three zone-centered librational lattice frequencies of species $E_g + 2T_g$, and relative intensities of these three

modes are shown in Fig. 5. The weak line observed on the shoulder of the librational line at 131 cm^{-1} is a grating ghost. The measured band positions shown in Table 1 are seen to be in good agreement with previously published results.

The Raman lattice bands were observed to be temperature dependent in the range of 18 to 83 K and to have large intensities relative to those of the intramolecular vibrations. As can be seen from Table 1, the frequency of the peak of the band of all three lattice vibration increases with decreasing temperature. Most prominent is the approximately three-percent increase in frequency in the 91.7-cm^{-1} line upon a temperature change of 65 K. Regarding the variation of the bandwidths with temperature, no change in the full widths at half maximum (FWHM) of the bands were observed. These observations are consistent with the results of both Cahill and Leroi (Ref. 15) and Cahill, et al. (Ref. 17).

In addition to the lattice modes of CO_2, Raman scattering from the intramolecular vibrations of CO_2 was also observed, and the band locations of 1278.0 and 1387.6 cm^{-1} were determined. These results are in reasonably good agreement with those of Cahill and Leroi (Ref. 15) who determined the band positions to be 1,277 and 1,385 cm^{-1}, respectively. It is to be noted that these two intramolecular vibrational Raman bands correspond to Stokes scattering processes involving the lowest-lying Fermi-resonance doublet of CO_2. Specifically, the 1278.0-cm^{-1} band corresponds to the molecular transition $(0,0°,0) \rightarrow (0,2°,0)$, and the 1387.6-cm^{-1} transition $(0,0°,0) \rightarrow (1,0°,0)$, where (v_1, v_2^{ℓ}, v_3) devotes the vibrational quantum numbers of the symmetrical stretch, deformation, and asymmetrical stretch vibrational modes, respectively; superscript ℓ designates the vibrational angular momentum quantum number. In support of the previously made assertion that for weakly bound crystals the intramolecular vibrational frequencies differed but little from the gas-phase values, it is noted that the gas-phase frequencies corresponding to the solid-state values of 1278.0 and 1387.6 cm^{-1} are 1285.5 and 1388.3 cm^{-1}, respectively (Ref. 18). These wave number changes between the gas and solid-state phases of less than one percent show clearly the utility of gas-phase Raman band locations for species identification of solid-state cryodeposits.

Concerning spectral interferences as a result of either Raman scattering or fluorescence, or both, from the sample substrate and trace impurities, all spectral scans exhibited Raman bands which were attributed to the Ge substrate. However, the location and intensities of the bands were such as to provide no spectral interference with the Raman bands of the cryodeposits. Further, no fluorescence from the substrate was observed, and so long as cleanliness was maintained for the deposition process no fluorescence resulted from trace impurities. However, on known occasions where such cleanliness was not maintained, Raman bands from both diffusion pump oil and vacuum grease were observed, but, even on those occasions, cryodeposit species identification by Raman scattering was still possible.

Of particular concern throughout the study was the possibility of the heating of the sample and its subsequent degradation by the incident laser beam. All cryodeposit samples appeared transparent after deposition at both 18 and 88 K, and no appreciable laser beam absorption or sample heating effects were encounted for incident laser powers less than 200 mW at wavelengths of either 5,145 and 4,880 Å. For such power levels, it was possible to maintain a constant substrate temperature, and repeated scans of both the lattice and intramolecular regions revealed no appreciable change in the sample as evidenced by the Raman scattering profiles. However, for laser beam incident power levels of 500 to 1,000 mW at 5,145 Å, laser heating of the cryopdeposit sample and subsequent sample loss were observed for N_2, NH_3, and H_2O.

Referring to the results shown in Table 1, it is seen that the measured Raman band positions for all species studied are in good agreement with results published previously. Further, the Raman spectra of cryodeposits of the pure samples of CO, N_2, and O_2 are known to exhibit a strong dependence on temperature (Ref. 15); however, the scope of this work did not extend to an investigation of this feature of the spectra. Finally, it is to be noted that at present the temperature dependencies of the Raman spectra of NH_3 and solid H_2O are not known.

4.2 Discrete Particle and Bulk Sample Results

The Raman spectrum scattering was obtained from a single polystyrene latex sphere $0.220 \mu m$ in diameter. The observed spectrum, whose line positions are recorded in Table 2, exhibited only the strongest characteristic bands of polystyrene (Ref. 19). A pronounced background level limited the quality of the spectra obtained from these samples, and significant background signal resulted from the glass substrate sample holder. However, sample heating of the polystyrene sphere was observed for all incident laser beam power levels as low as 100 mW, and fluorescence from impurities in the polystyrene microsphere is a possible contributor to the background signal.

In addition to single particle Raman scattering, the Raman scattering spectra of bulk, powdered samples of inorganic particles were also obtained. Samples of ammonium nitrate (NH_4NO_3) and sodium nitrate ($NaNO_3$) were selected for study for the following reasons: (1) the Raman spectra of these species were relatively simple with reasonably intense major bands; (2) no appreciable visible absorption or fluorescence by these species was known to exist; (3) both species were expected to exhibit strong temperature-dependent spectral features, thereby enabling the detection of any significant sample heating and providing the opportunity to demonstrate the ability for a temperature measurement of the sample; and (4) the ease of sample handling and storage.

A representative spectrum of $NaNO_3$ is presented in Fig. 6, and spectral features common to the Raman profiles of both species are well illustrated by the results of Fig. 6. For both samples, the region below 300 cm^{-1} exhibits a strong wing of the elastic scattering peak and widely separated, intense characteristic intramolecular vibrational bands. Sodium nitrate belongs to the space group D_{3d}^5, and the Raman active phonon mode assignments along with observed lines are listed in Table 3. (Also included in Table 3 are the assignments for the NH_4NO_3 sample.) These observations are in good agreement with those of prior studies (SRef. 19). No significant sample heating was evident from any spectra that have been observed from either $NaNO_3$ or NH_4NO_3 sample. Since the molecular species studied were powdered, bulk samples contained in a specially constructed sample holder, as expected, no spectral interference from either the sample support mechanism or the temperature measurement devices was encountered.

Considering the potential applications of the Raman scattering technique to contamination studies, it is of considerable interest to determine the possible use of Raman scattering for detecting changes in the relative mole fractions in a mixture sample. To evaluate the feasibility of the technique for performing such measurements, binary mixture samples of $NaNO_3$-NH_4NO_3 were prepared using the method outlined in a previous section, and the relative concentration of $NaNO_3$ was varied systematically from zero to 100 percent. The complete Raman spectrum for each sample of different composition was recorded at room temperature and the resulting Raman profiles compared. The results of these comparisons for selected bands are presented in detail in Figs. 7 through 9. The variation with sample mole fraction of the Raman intensity of the observed bands is apparent in Figs. 7 through 9. As the mole fraction for a given component increases (decreases), the Raman intensity for the given band also increases (decreases). No apparent change in the FWHM of the bands was noted. Although difficulty was encountered in extracting useful information from some of the spectral bands as a result of spectral overlap, most bands allowed an unambiguous determination of the variation of their intensity values with concentration changes.

To quantify the spectral variations as a function of change in concentration of the sample, a ratio was formed from the product of the peak intensities (and half widths) of the 724 cm^{-1} and 1,068^{-1} bands of $NaNO_3$ in the mixture and those of the 714 cm^{-1} and 1,042 cm^{-1} bands of NH_4NO_3. The dependence of this ratio on concentration is presented in Fig. 10. Since these sample mixtures were formed by a simple combination of pure, powdered samples, no intermolecular interaction was expected since the resulting sample volume contains only a mixture of randomly oriented particles. It was observed that no changes occurred in the lattice mode region of the Raman profiles as the sample mixture concentration was varied, and this result supports the assertion of randomly oriented

particles. As a result of the absence of significant interaction between the two species of the mixture, the concentration dependence of the intensity ratio shown in Fig. 10 is simply behaved, and this simple behavior is expected to be similar to that to be encountered in unreacting cryodeposit mixtures which can occur in certain contamination applications. For reacting or strongly interacting species in a cryodeposit mixture, deviation from this simple behavior is to be expected. Finally, an investigation was also performed of the dependence of the Raman spectrum on the variation of sample temperature. A strong dependence on temperature was observed for both the peak intensity and the FWHM linewidth for the 1,068-cm^{-1} mode of $NaNO_3$. An increase in peak intensity by a factor of approximately four was observed upon decrease in sample temperature from 531 K to 295 K for this mode. Further, the Raman scattering band intensities at 185 cm^{-1}, and 724 cm^{-1}, remained essentially constant over this temperature range, whereas the 98 cm^{-1} band exhibited a decrease in intensity of approximately 20 percent in frequency and the 1,383-cm^{-1} line by approximately one percent as the temperature increased from 295 K to 531 K. As a simple illustration of this strong temperature dependance, Fig. 11 presents the variation in intensity of the 1,068-cm^{-1} line of $NaNO_3$ with sample temperature. Clearly, determination of the sample temperature is possible using the Raman spectrum.

5.0 SUMMARY OF RESULTS

The goal of this work was to demonstrate the feasibility of the application of Raman scattering diagnostics to cryodeposit and contamination studies. To this end, a series of measurements was performed using cryogenically cooled cryodeposit samples of single molecular species. The samples were formed by comparatively slow deposition of a nominally effusive molecular beam onto a cold Ge substrate. The Raman data acquired from such samples exhibited both the lattice mode and intramolecular vibrational mode structures which are characteristic of weakly interacting molecular structures. These spectral features associated with the molecular species and their structures showed clearly the ability of Raman scattering to determine the identity of such solid-state species. Further, limited measurements of the temperature variation of the location and shape, or width, of the Raman bands provided an indication of the possibility and approach to be followed to effect a temperature determination of such a cryodeposit.

Recognizing the existence of contaminating, adsorbed particulates, in constant to quasi-continuous cryodeposit layers, an experimental study was performed to demonstrate the feasibility of single particle Raman scattering. Scattering was observed from a 0.220-μm-diam polystyrene microsphere, and the Raman spectra characteristic of polystyrene was observed. Additionally, a laser-induced background signal was also observed which degraded the Raman scattering signal-to-noise ratio but did not preclude successful Raman

measurements. Moreover, although not explored in this limited study, if the laser-induced background signal can be attributed to fluorescence of an impurity present in the polystyrene, an additional method of species identification exists.

Finally, to demonstrate the feasibility of relative species concentration and temperature measurements using Raman scattering, studies were performed on binary mixtures of powdered, bulk samples of NH_4NO_3 and $NaNO_3$. The results of these measurements showed clearly the feasibility of such measurements using the observed intramolecular vibrational bands of the individual species.

REFERENCES

1. Long, D. A. *Raman Spectroscopy*. McGraw-Hill International Book Co., New York, 1977.

2. Born, M. and Huang, K. *Dynamical Theory of Crystal Lattices*. Oxford at the Clarendon Press, 1956.

3. Wilkinson, G. R. "Raman Spectra of Solids." *Molecular Spectroscopy*, Vol. 3, ed. Barrow, R. F., Long, D. A., and Milleu, D. J. The Chemical Society, Burlington House, London, 1975, pp. 433-496.

4. Duncan, I. and Stewart, J. H. *Light Scattering in Solids*. ed. Balkanshi, M., Flammarian, Paris, 1971, p. 308.

5. Bobovich, Ya. S. and Tulub, T. P. *Optika i Spektroskopiya*, Vol. 6, 1959, p. 566.

6. Rao, A. D. P., Katiyar, R. S., and Porto, S. P. S. "Temperature Dependent Raman Scattering in Sodium Nitrate.", *Advances in Raman Spectroscopy*, Vol. 1, ed. Mathieu, J. P., Heyden and Son, LTD., London, 1972.

7. Mitra, S. S., Brafman, O., Daniels, W. B., and Crawford, R. K. "Pressure-Induced Phonon Frequency Shifts Measured by Raman Scattering." *Physical Review*, Vol. 186, No. 3, 1969, pp.942-944.

8. Korshunov, A. V. and Bondarev, A. F. *Optika i Spektroskopiya*, Vol. 15, 1963, p. 182.

9. Sushchinskii, M. M. *Raman Spectra of Molecules and Crystals*. Israel Program for Scientific Translations, New York, 1972.

10. Sushchinskii, M. M. "The Intensity of the Dispersion Rays (Raman Spectra) Caused by Molecular Linkages in Solutions, as a Function of Their Concentrations." Doklady, A. N. SSSR, 33, 1941, pp. 18 -21.

11. Chang, I. F. and Mitra, S. S. "Application of a Modified Random-Element-Isodisplacement Model to Long-Wavelength Optic Phonons of Mixed Crystals." *Physical Review*, Vol. 172, No. 3, 1968, pp. 924-933.

12. Roux, J. A., Wood, B. E., and Smith, A. M. "IR Optical Properties of Thin H_2O, NH_3, and CO_2 Cryofilms." AEDC-TR-79-57 (A074913), September 1979.

13. Tempelmeyer, K. E., and Mills, D. W., Jr. "Refractive Index of Carbon Dioxide Cryodeposit." *Journal of Applied Physics*, Vol. 39, No. 6, May 1968, pp. 2968-2969.

14. Williams, W. D. and Lewis, J. W. L. "Rotational Temperature and Number Density Measurements of N_2, O_2, CO, and CO_2 in a Hypersonic Flow Field using Laser-Raman Spectroscopy." AEDC-TR-75-37 (ADA012877), July 1975.

15. Cahill, J. E. and Leroi, G. E. "Raman Spectra of Solid CO_2, N_2O, N_2, and CO." *Journal of Chemical Physics*, Vol. 51, No. 4, 1969, pp. 1324-1332.

16. Bhagavantam, S. and Venkatarayudu, T. *Theory of Groups and Its Application to Physical Problems*. Academic Press, New York, 1969.

17. Cahill, J. E., Treuil, K. L., Miller, R. E., and Leroi, G. E. "Raman Spectra of Polycrystalline CO_2 and N_2O." *Journal of Chemical Physics*, Vol. 47, 1967, pp. 3678-3679.

18. Herzberg, Gerhard *Spectra of Diatomic Molecules*. Van Nostrand Reinhold Company, New York, 1950.

19. Rosasco, G. J., Etz, E. S., and Cassatt, W. A. "The Analysis of Discrete Fine Particles by Raman Spectroscopy." *Applied Spectroscopy*, Vol. 29, No. 5, 1975, pp. 396-404.

20. Cahill, J. E., and Leroi, G. E. "Raman Studies of Molecular Motion in Condensed Oxygen." *Journal of Chemical Physics*, Vol. 51, No. 1, July 1969, pp. 97-104.

21. Cabana, A., Anderson, A., and Savoie, R. "Raman Spectrum of CH_4 Trapped in Solid Krypton. Evidence for Molecular Rotation." *Journal of Chemical Physics*, Vol. 42, No. 3, February 1965, pp. 1122-1123.

22. Bondybey, Vladimir E. and Nibler, Joseph W. "Infrared and Raman Spectra of Solid and Matrix Isolated Diimide, HNNH." *Journal of Chemical Physics,* Vol. 58, No. 5, March 1973, pp. 2125-2134.

23. Cornell, S. W. and Koenig, J. L. "Laser-Excited Raman Scattering in Polystyrene." *Journal of Applied Physics,* Vol. 39, No. 11, October 1968, pp. 4883-4890.
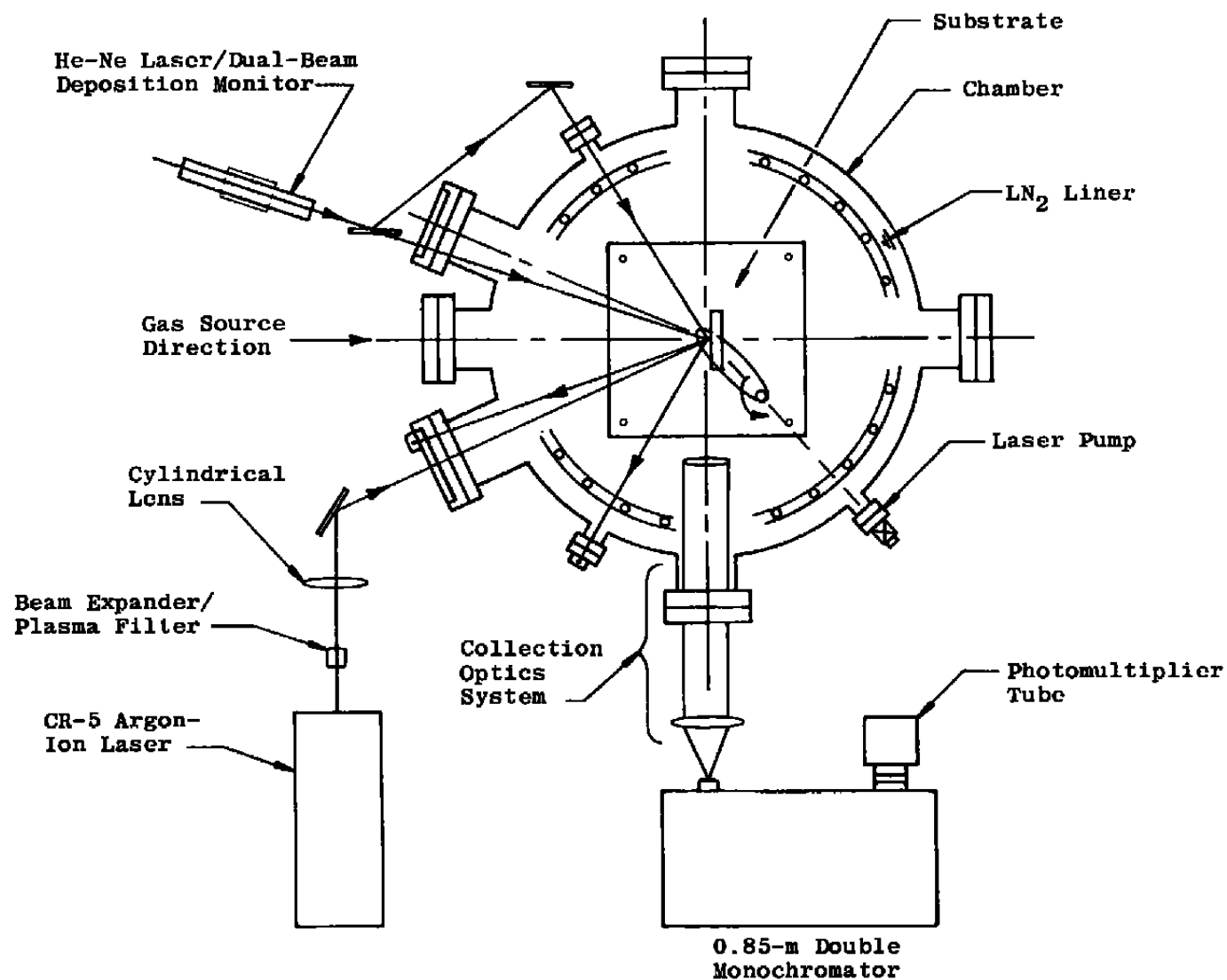
He-Ne Laser/Dual-Beam
Deposition Monitor

Substrate

Chamber

LN_2 Liner

Gas Source
Direction

Laser Pump

Cylindrical
Lens

Beam Expander/
Plasma Filter

CR-5 Argon-
Ion Laser

Collection
Optics
System

Photomultiplier
Tube

0.85-m Double
Monochromator

Figure 1. Low-temperature Raman scattering experimental system.

1. Effusive beam, 38-mm-diameter (1.5.).
2. Optical stop required to underfill cryocooled window with effusive beam. Also, this stop is supported by a 3-in. -ID pipe that prevents gas added to chamber from cryopumping on rear of substrate.
3. Aluminum holder with cryogenic passageways.
4. Germanium window heat sunk with an indium gasket to the aluminum holder.
5. Cover plate.
6. Gaseous helium or liquid nitrogen inlet.
7. Gaseous helium or liquid nitrogen outlet.
8. Crosshatched area illustrates area of window heat sunk to holder. Clear diameter is 50.7 mm (2 in.) while infrared beam diameter is 38 mm (1.5 in.).
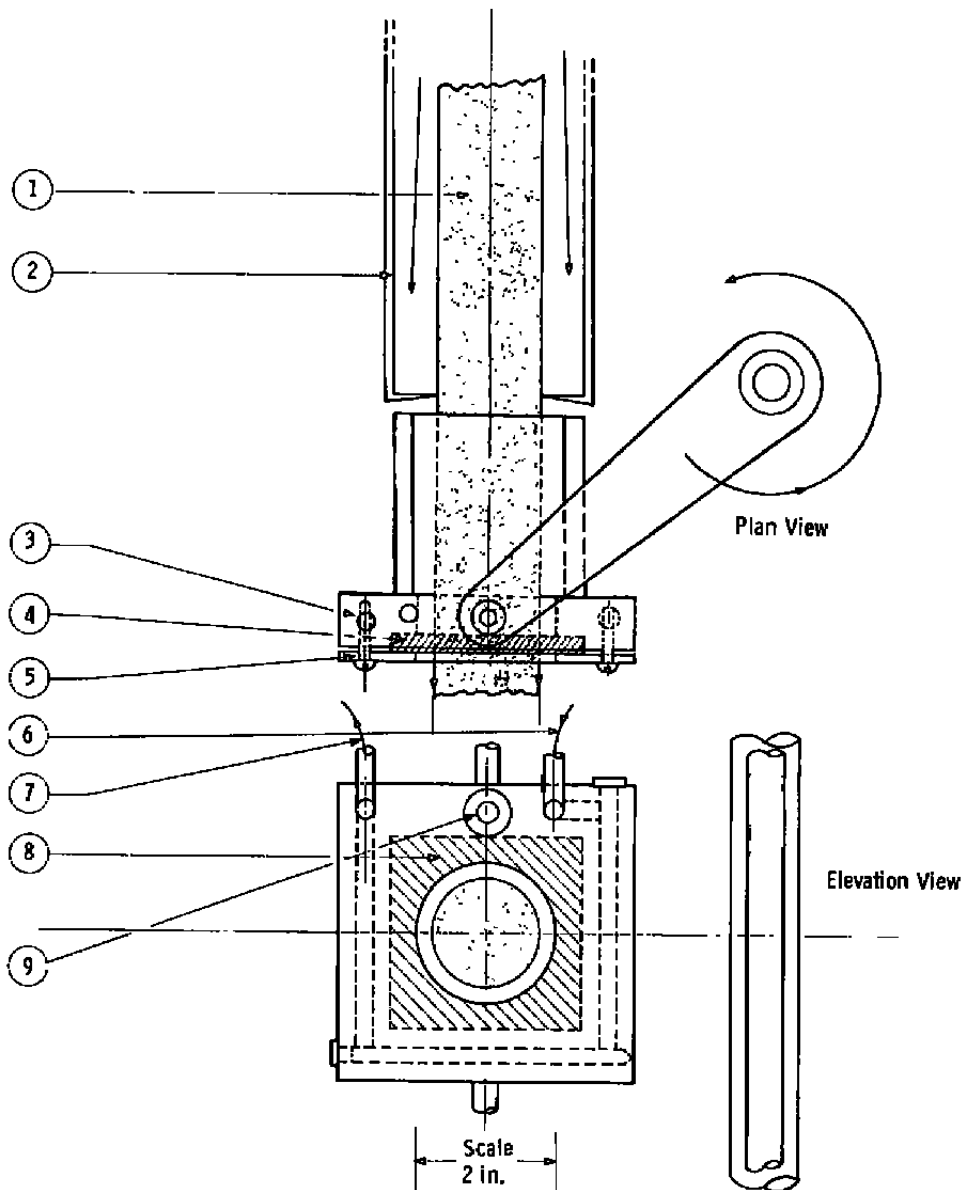9. QCM heat sunk with indium gasket to aluminum holder.

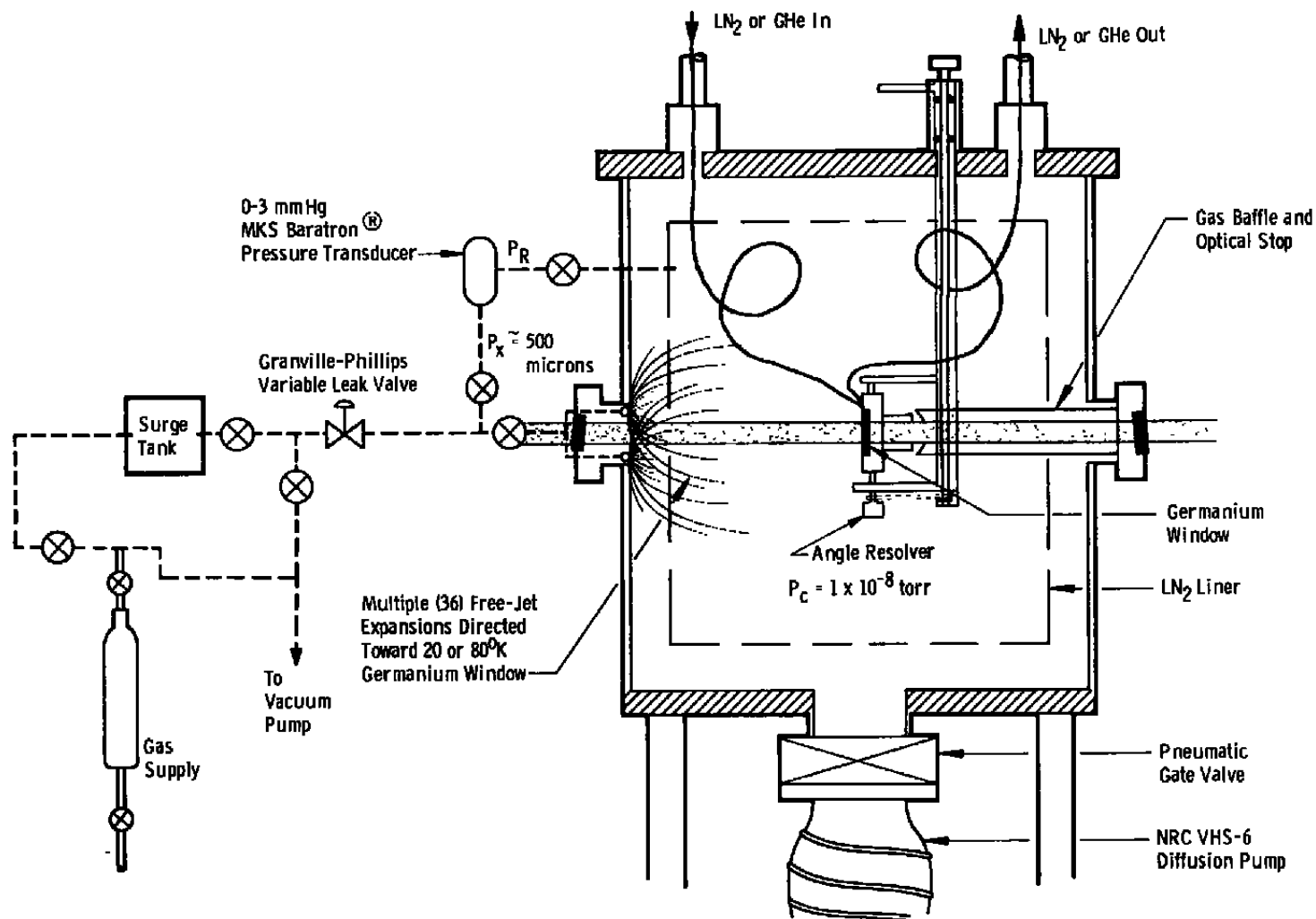Figure 2. Plan and elevation views of cryogenically cooled substrate holder.

LN$_2$ or GHe In

LN$_2$ or GHe Out

0-3 mmHg
MKS Baratron®
Pressure Transducer

P_R

Gas Baffle and
Optical Stop

$P_x \cong 500$ microns

Granville-Phillips
Variable Leak Valve

Surge
Tank

Multiple (36) Free-Jet
Expansions Directed
Toward 20 or 80°K
Germanium Window

To
Vacuum
Pump

Gas
Supply

Angle Resolver

$P_c = 1 \times 10^{-8}$ torr

Germanium
Window

LN$_2$ Liner

Pneumatic
Gate Valve

NRC VHS-6
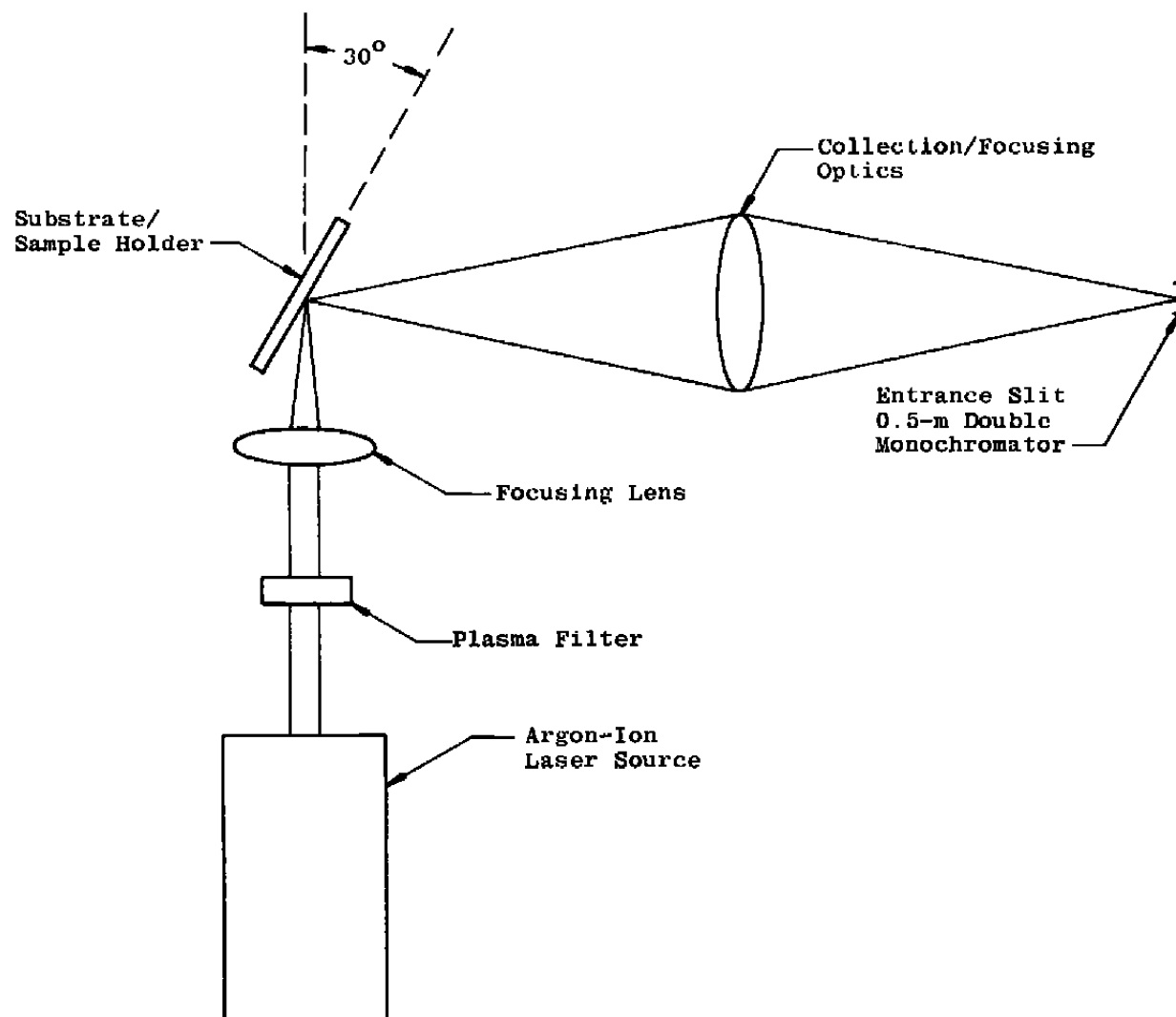Diffusion Pump

Figure 3. Gas deposition system.

Figure 4. Temperature/concentration Raman scattering system.
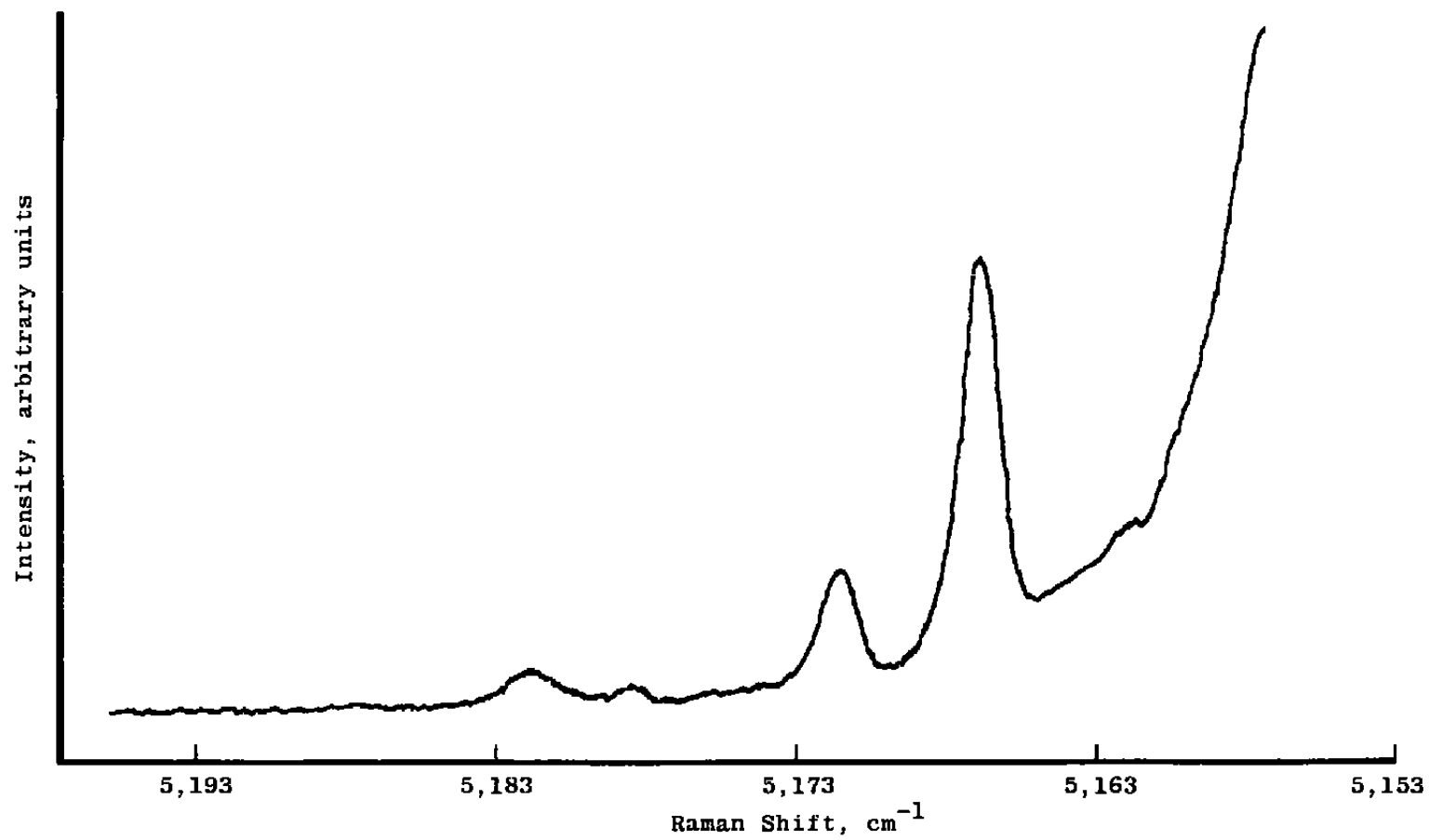
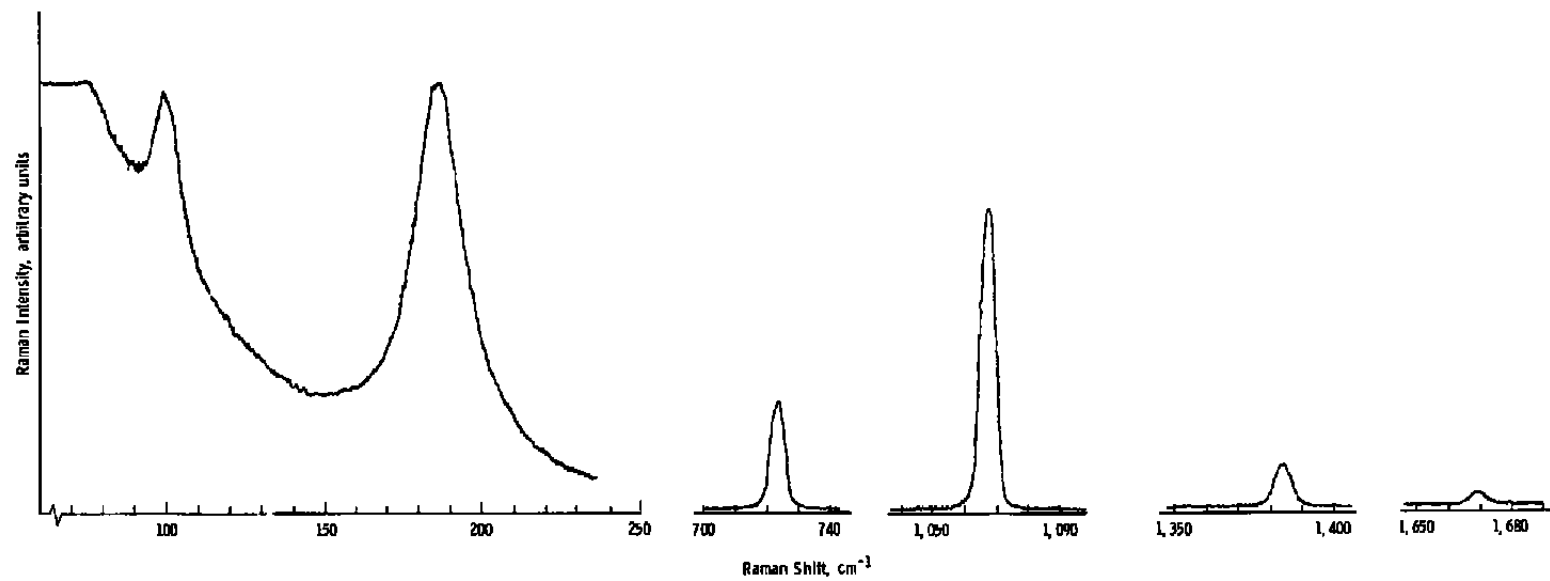Figure 5. Raman spectrum of lattice mode region of condensed CO_2, 83 K.
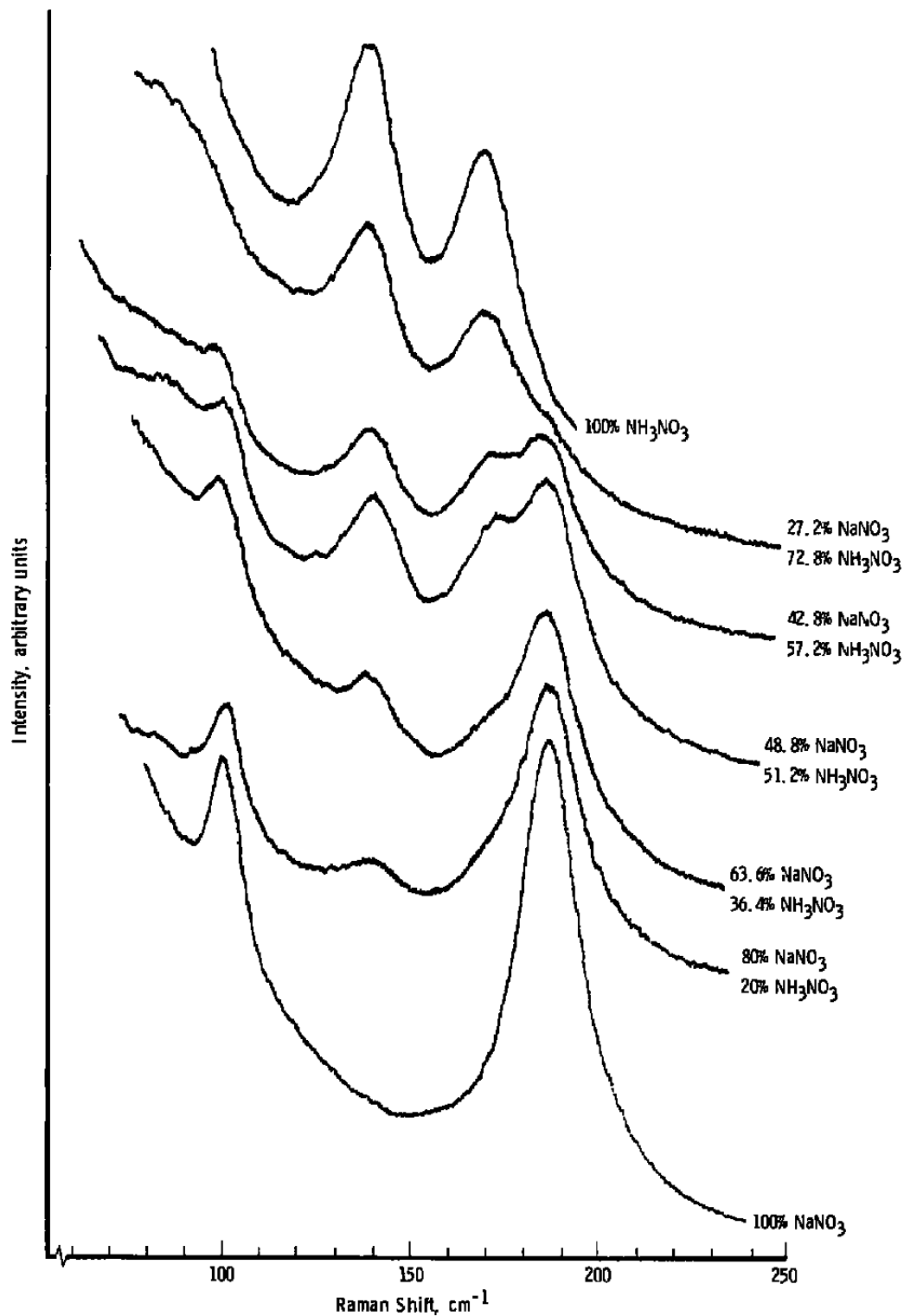
Figure 6. Raman spectrum of sodium nitrate, NaNO₃.

Figure 7. Variation of Raman spectra under concentration variation:
sodium nitrate — ammonium nitrate mixture, 50 to 250 cm⁻¹
region.
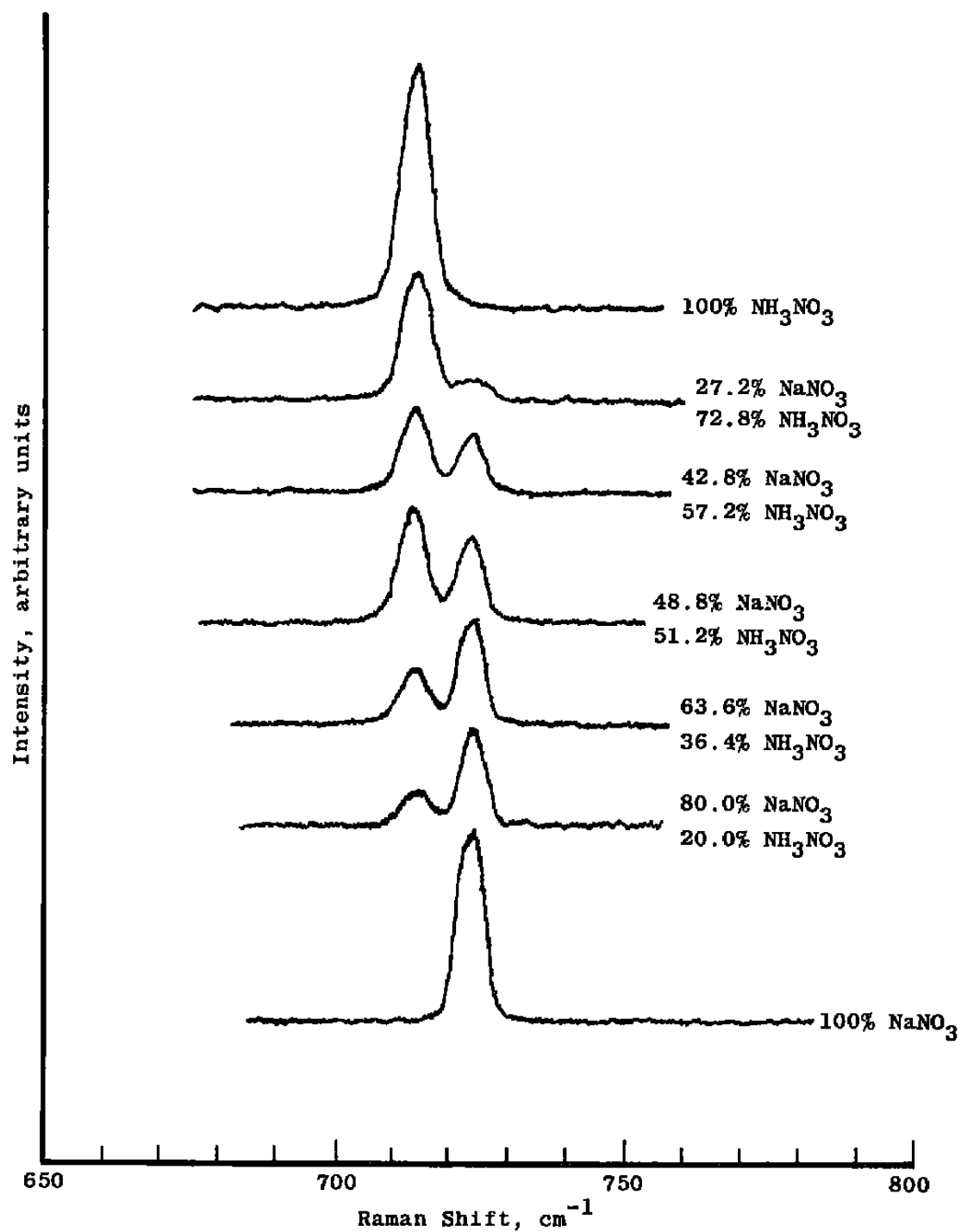
Figure 8. Variation of Raman spectra under concentration variation: sodium nitrate — ammonium nitrate mixture, 650 to 800 cm⁻¹ region.
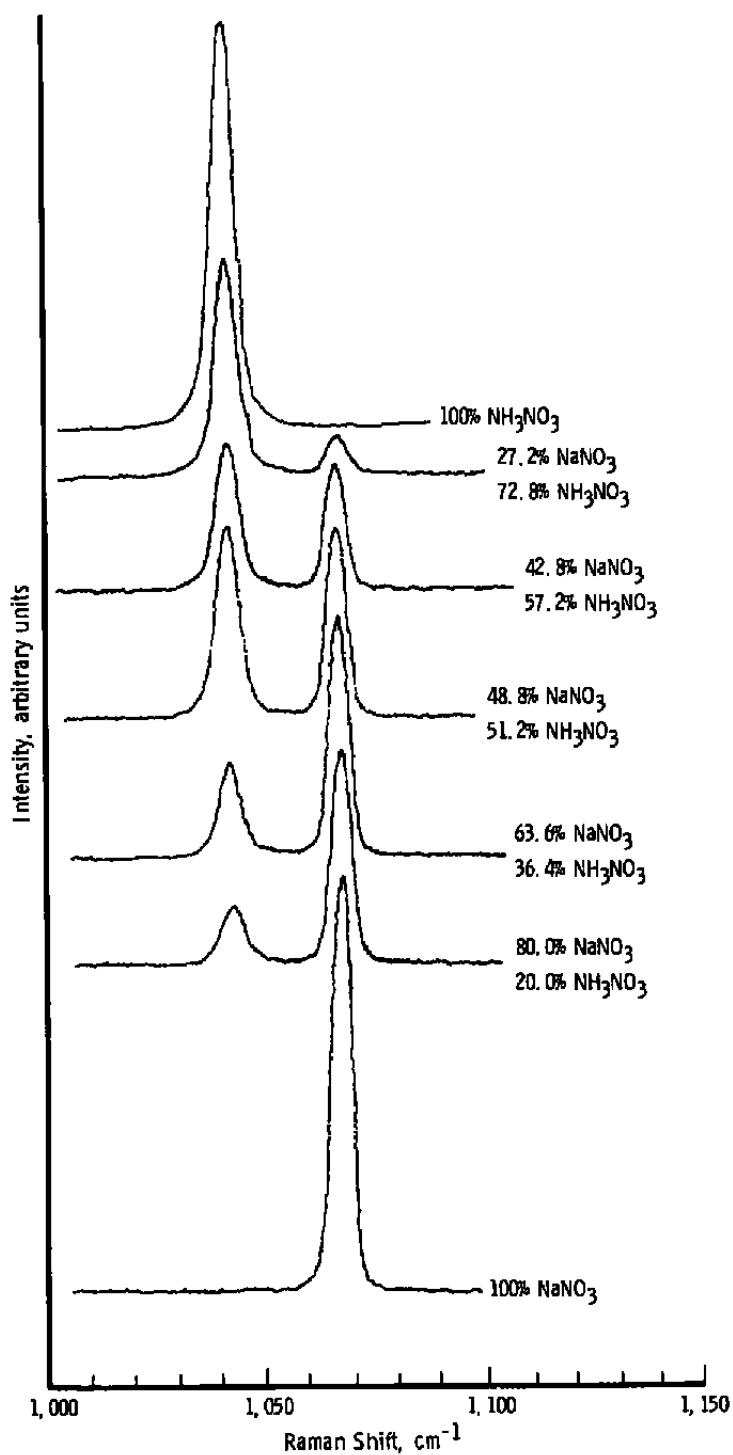
Figure 9. Variation of Raman spectra under concentration variation: sodium nitrate — ammonium nitrate mixture, 1,000 to 1,100 cm^{-1} region.
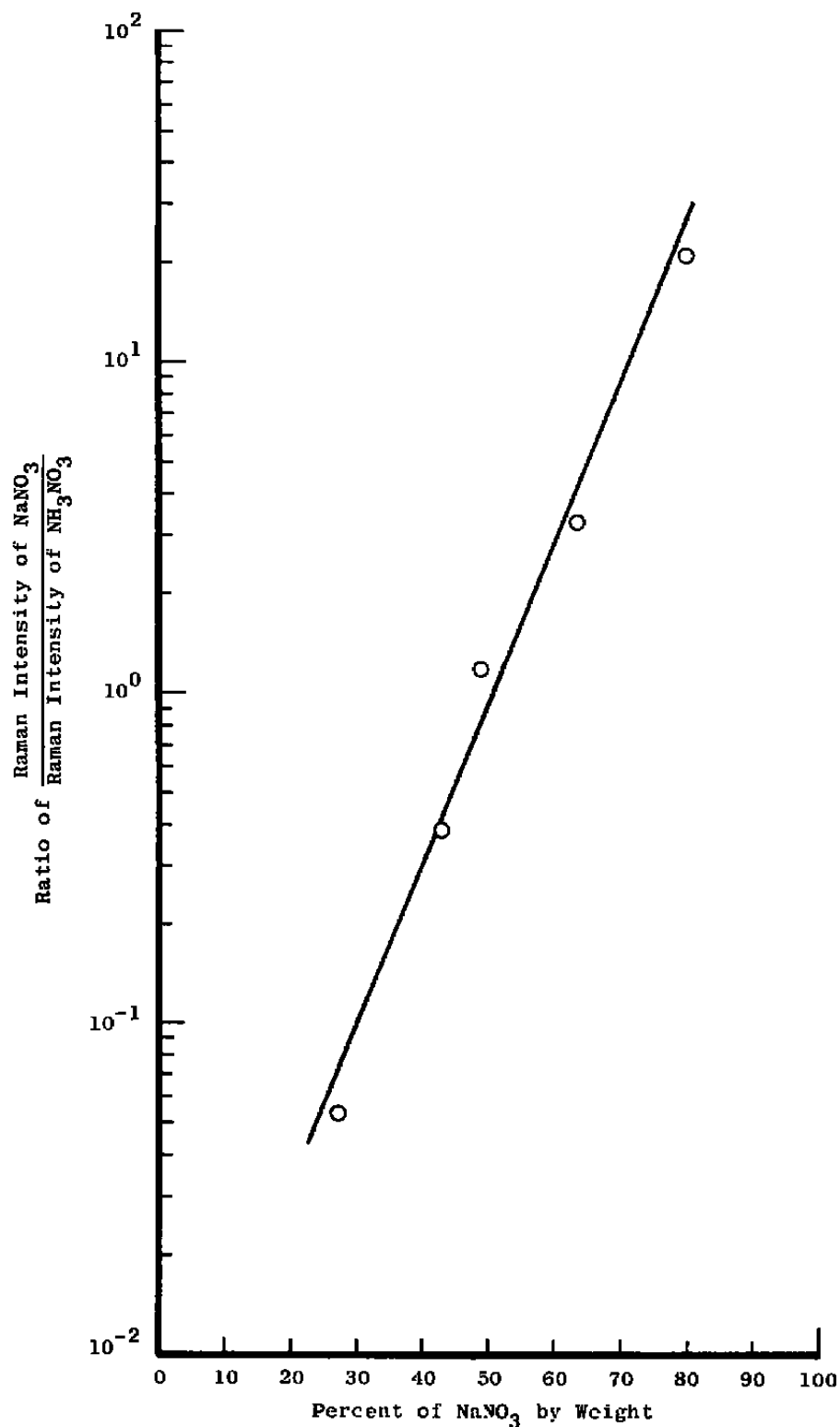
Figure 10. Variation of Raman intensity ratio as a function of concentration in an $NaNO_3$-NH_4NO_3 mixture.
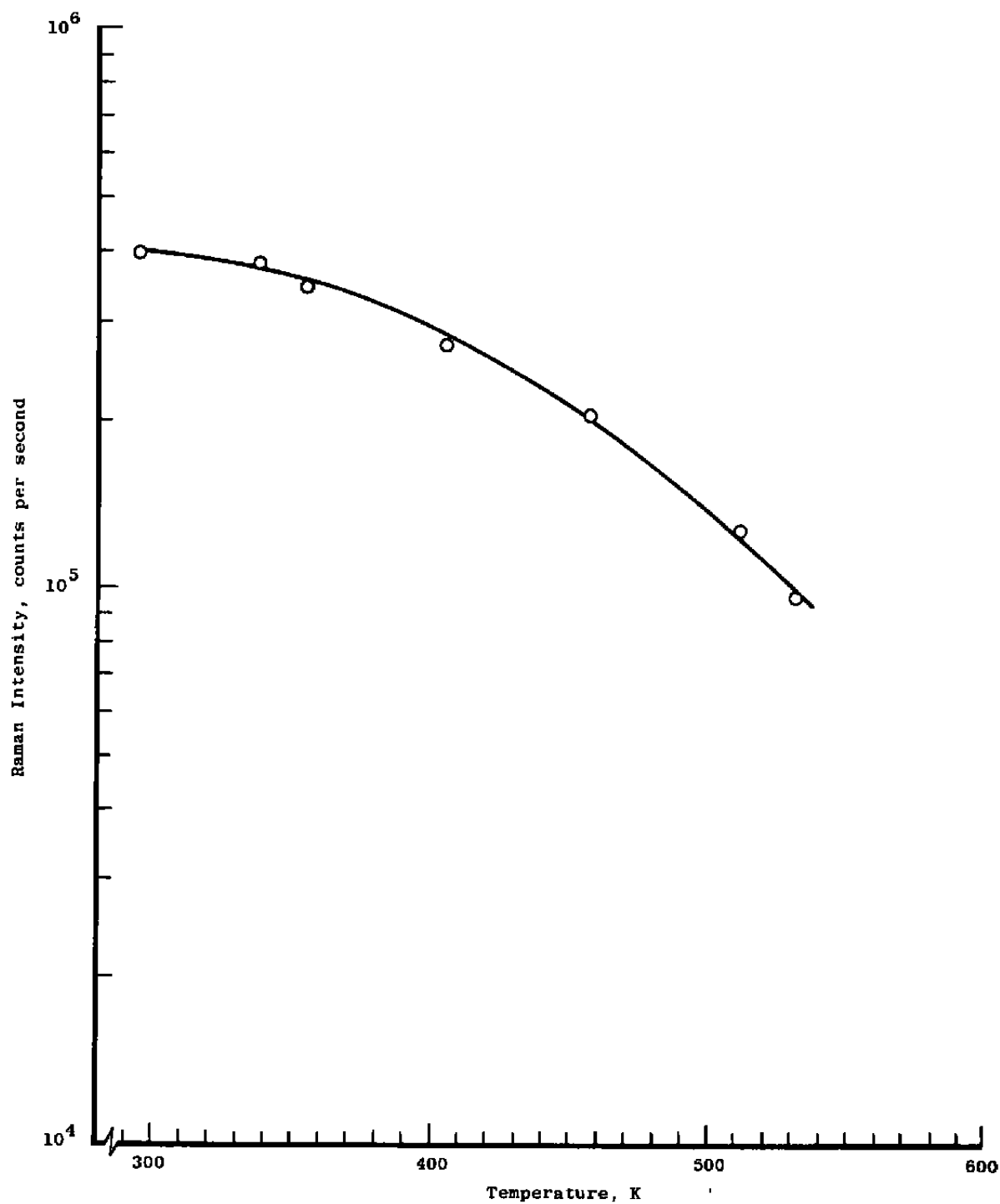
34

Figure 11. Variation of Raman intensity of 1,068 cm⁻¹ internal
mode of NaNO₃ with temperature.

Table 1. Ramam Band Locations — Cryodeposit Samples

Cryodeposit	Temperature, K	Frequency, cm^{-1}	Prior Study (Refs. 15, 17, 18, 20, 21, and 22)	
			Temperature, K	Frequency, cm^{-1}
CO_2	18.0	74.3		
	18.0	94.9		
	18.0	131.3		
	83.0	73.9	81	73.0
	83.0	91.7	81	90.5
	83.0	129.0	81	131.0
	83.0	1278.0	88	1277.0
	83.0	1387.6	88	1385.0
CO	17.0	2141.6	30	2140.0
N_2	21.2	2321.8	18	2329.0
O_2	21.5	71.0	22	78.0
	21.5	1552.7	22	1552.5
CH_4	21.0	2908.0	13	2912.0
NH_3	82.7	1131.1	12	1115.0
	82.7	3239.6	12	3213.0
	82.7	3278.3	12	3293.0
	82.7	3373.5	12	3375.0
H_2O	83.0	3069.0	88	3089.3
	83.0	3712.32	390	3134.3

Table 2. Ramam Band Locations — Polystyrene Sample

Frequency, cm^{-1}	Assignment	Prior Study (Ref, 23) Frequency, cm^{-1}
620.0	B$_1$	615.0
1000.5	A$_1$	997.0
1153.5	B$_1$	1148.0
1202.3	A$_1$	1198.0
1600.0	B$_1$	1593.0

Table 3. Raman Band Assignments — Bulk Samples

Observed Raman Shift, cm^{-1}		Assignment
NaNO$_3$	NH$_4$NO$_3$	
98	---	E$_g$, External mode, translation
185	140	E$_g$, External mode, libration
724	714	E$_g$, Internal mode, in-plane bend
1,068	1,042	A$_g$, Internal mode, symmetric sketch
1,383	---	E$_g$, Internal mode, asymmetric sketch

NOMENCLATURE

A,B,C	Compound designators
c	Volume concentration
$\vec{E}$	Electric field vector
E	Electric field amplitude
$\lvert f \rangle$	Final state wave function
$g(\nu,\nu')$	Function of incident and scattered frequencies
H	Total Hamiltonian
H_L	Lattice component of Hamiltonian
H_v	Intramolecular component of Hamiltonian
$\hbar$	$h/2\Pi$
h	Planck constant
I	Scattering intensity
$\lvert i \rangle$	Initial state wave function
K	Constant of proportionality
k_B	Boltzmann constant
$\vec{P}$	Polarization vector
$\lvert Q \rvert$	Normal coordinates or displacement vectors
RS	Spontaneous Raman scattering
S	Constant of proportionality
T	Temperature, K
$\underline{\alpha}$	Polarizability tensor
Γ	Raman line half width
Δ	Raman line shift in frequency
λ	Wavelength of radiation

ν	Frequency of radiation
Π	Product operator
x	Concentration fraction
$|\Psi|$	Total eigenfunction
ω	Scattered photon wave number

SUBSCRIPTS

o	Incident equilibruim
A,B	Component designators
ℓ	Denotes lattice mode
ν	Denotes intramolecular vibrational mode
x	Concentration fraction

SUPERSCRIPTS

ℓ	Denotes lattice mode
v	Denotes intramolecular vibrational term